A Blocker-Tolerant mm-Wave MIMO Receiver with Spatial Notch Filtering Using Non-Reciprocal Phase-Shifters for 5G Applications

Shahabeddin Mohin, Soroush Araei, Mohammad Barzgari, Negar Reiskarimian
Massachusetts Institute of Technology, USA
negarr@mit.edu

***Abstract*— This work reports a highly-linear blocker-tolerant mm-wave MIMO receiver front-end for 5G and beyond-5G applications. The proposed architecture enhances the RX linearity performance by establishing a mm-wave spatial notch filter (SNF) at the LNA output. The SNF incorporates a low-loss non-reciprocal phase-shifter architecture that can be turned off in the absence of spatial blockers. A 27-31GHz four-element MIMO receiver prototype is implemented in a 45nm SOI technology and exhibits an in-notch IP1dB of -7.8dBm with up to 41dB spatial blocker rejection. Through significant cancellation of co-channel wideband blockers, the RX achieves an EVM of -32.6dB, while receiving a wideband 256-QAM 100MS/s desired signal.**

***Keywords*— 5G, blocker-tolerant, digital beamforming, mm-wave, multiple-input multiple-output, MIMO, nonreciprocal phase-shifter, spatial notch filter.**

I. Introduction

Mm-wave beamforming receivers (RX) have gained widespread popularity due to their potential for increasing spectral efficiency, signal-to-noise ratio and supporting multiple-input multiple-output (MIMO) operation. Analog beamformers provide spatial blocker suppression within the RX front-end, hence, protecting the analog-to-digital converter (ADC) from being exposed to large blocker signals. Digital beamformers on the other hand, are susceptible to large signal interference and require high RX/ADC dynamic range and linearity to prevent saturation. To mitigate this issue, many techniques have been introduced in the literature [1], [2], [3], [4] to create spatial notch filters that selectively reject interference from one or more specific incident angles.

Sub-6GHz receivers such as [1] take advantage of the impedance translation feature of passive mixers to transform a baseband spatial notch impedance to RF. This approach cannot be applied directly at mm-wave frequencies due to the degradation of passive mixer performance at higher frequencies. For mm-wave systems, cascadable SNF architectures have been demonstrated that can be employed either at mm-wave [2] or intermediate frequency (IF) [2], [3]. In these architectures any RX blocks preceding the SNF, phase-shifters (PSs) and buffers/variable gain amplifiers especially those within the first-stage of SNF, are prone to large signal blockers, hence degrading RX linearity. Another approach demonstrated in [4] (Fig. 1(a)), utilizes active PSs in the main paths and passive bi-directional all-pass filters in auxiliary paths that connect to a central node to perform destructive interference of spatial blockers. This approach improves RX linearity by rejecting the interferers at PS outputs (-14dBm in-notch IP1dB compared to -19dBm in [3]).

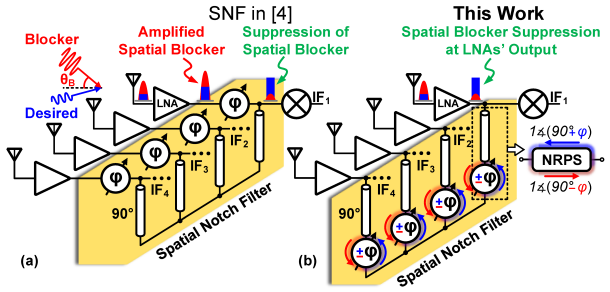

Fig. 1. (a) Spatial notch filtering approach introduced in [4], and (b) the proposed technique using non-reciprocal phase-shifters.

Fig. 1(b) illustrates the proposed highly-linear SNF architecture supporting N-input-N-output MIMO systems. Our approach uses low-loss nonreciprocal phase-shifters (NRPSs) designed to suppress spatial blockers directly at the low noise amplifier (LNA) outputs, providing an opportunity to target blockers at the earliest point within the RX. Compared to [4], this structure provides the following benefits: (I) It improves the RX linearity by rejecting the blockers at the LNA outputs, achieving -7.8dBm in-notch IP1dB. (II) It allows the SNF to be fully turned off in the absence of spatial interferers, lowering power consumption and noise contributions of the SNF circuitry.

II. Spatial Notch Filter Using NRPS

In the proposed highly-linear SNF architecture (Fig. 1(b)), the outputs of the LNAs are protected from large spatial blockers, thus avoiding LNA saturation. To understand the design requirements of such architecture, we consider the G matrix, defined as the gain from each antenna input to where blocker cancellation happens in each path (output of PS in Fig. 1(a), G_{1a} or LNA output in Fig. 1(b), G_{1b}). For a blocker incident at an angle of θ_B, the antenna inputs for a 4-element linear array are shown in Fig. 2. To perfectly cancel the blockers in Fig. 1(a) at each PS output, G should be configured as follows:

$$G_{1a} = A_v \begin{bmatrix} 1 & -\frac{1}{3} & -\frac{1}{3} & -\frac{1}{3} \\ -\frac{1}{3} & 1 & -\frac{1}{3} & -\frac{1}{3} \\ -\frac{1}{3} & -\frac{1}{3} & 1 & -\frac{1}{3} \\ -\frac{1}{3} & -\frac{1}{3} & -\frac{1}{3} & 1 \end{bmatrix}, \quad (1)$$

where A_v is the LNA gain. The required G_{1a} is a symmetric matrix. However, to enable blocker rejection at the output of each LNA in our proposed architecture, it can be shown that the following G matrix is needed:

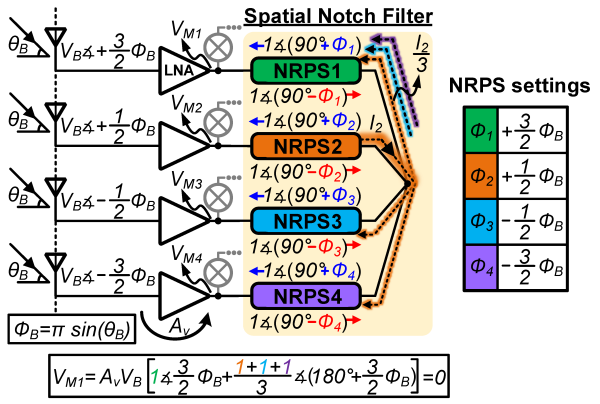

Fig. 2. Detailed operation of the proposed SNF.

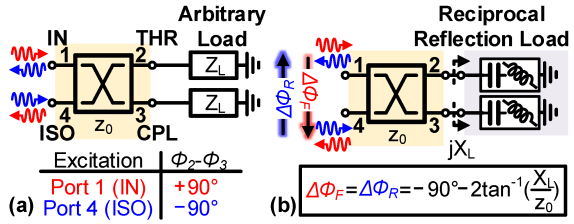

Fig. 3. (a) Phase difference between the THR and CPL ports in a hybrid coupler depending on the excitation port. (b) Reflection-type phase-shifter with reciprocal phase shift.

$$G_{1b}=A_v\begin{bmatrix}1 & -\frac{1}{3}e^{j\phi_B} & -\frac{1}{3}e^{j2\phi_B} & -\frac{1}{3}e^{j3\phi_B}\\ -\frac{1}{3}e^{-j\phi_B} & 1 & -\frac{1}{3}e^{j\phi_B} & -\frac{1}{3}e^{j2\phi_B}\\ -\frac{1}{3}e^{-j2\phi_B} & -\frac{1}{3}e^{-j\phi_B} & 1 & -\frac{1}{3}e^{j\phi_B}\\ -\frac{1}{3}e^{-j3\phi_B} & -\frac{1}{3}e^{-j2\phi_B} & -\frac{1}{3}e^{-j\phi_B} & 1\end{bmatrix}. \quad (2)$$

As can be seen, the G matrix in Eq. (2) is Hermitian. For example, the phase of G_{12} is $180°+\phi_B$, but the phase of G_{21} is $180°-\phi_B$, indicating a nonreciprocal behavior. *As a result, the cancellation of blockers within all paths is not achievable using the trivial reciprocal PSs used in [4].* Therefore, we propose using NRPSs to synthesize Eq. (2) to simultaneously reject blockers at all LNA outputs. Each NRPS has a phase of $90°\pm\phi_i$ in the reverse and forward directions, where ϕ_i can be controlled independently for $i=1:N$. Additionally, the NRPSs are placed in the auxiliary paths and can be turned off in the absence of spatial blockers, resulting in less power consumption and noise penalty.

A. Blocker-Cancellation Operation

Superposition theorem can be applied to calculate the voltage at the first LNA output. Assuming an incoming signal at the second antenna, the voltage contribution of this input at the output of the second LNA is $A_vV_B\angle+\frac{1}{2}\phi_B$. The forward phase shift introduced by NRPS2 is $90°-\frac{1}{2}\phi_B$, resulting in a current generated at the output of NRPS2 with a phase of $90°$. It can be demonstrated that the impedance looking from the common node into each NRPS is identical. As a result, $\frac{I_2}{3}$ flows through NRPS1, where I_2 represents the output current of NRPS2. Similarly, the currents flowing into NRPS1

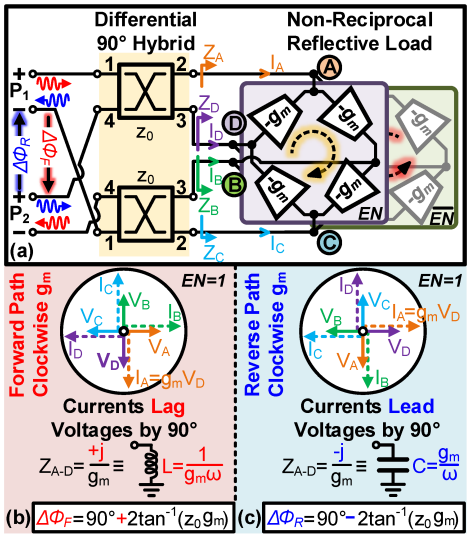

Fig. 4. (a) Circuit implementation of the NRPS. Equivalent loads for the clockwise set of g_ms in the: (b) Forward path, and (c) reverse path.

due to the inputs at the third and fourth antennas (I_3 and I_4) have a phase of $90°$ and add constructively with the second antenna's contribution. Furthermore, the total current fed into NRPS1 experiences an additional phase shift of $90°+\frac{3}{2}\phi_B$ in the reverse path of NRPS1 to create a voltage at the first LNA output. Finally, the collective effect of all of the input blocker signals cancel out at the output of the first LNA. This procedure is repeated for the other antennas, indicating that the blocker is effectively rejected at the output of each LNA.

B. NRPS Topology

Fig. 3(a) shows a traditional hybrid coupler with quadrature signals at the through (THR) and coupled (CPL) ports. As can be seen here, the phase difference between the THR and CPL ports can be either +90° or -90°, depending on if the signal is injected at the input (IN) or the isolation (ISO) port. A reciprocal reflection-type phase-shifter (RTPS) is built as seen in Fig. 3(b) by connecting the THR and CPL ports of the hybrid coupler to pure reactive (capacitive or inductive) loads.

The loss-less NRPS topology introduced here is depicted in Fig. 4(a), in which a differential hybrid coupler is connected to two sets of four transconductances (g_m) placed in a clockwise and counter-clockwise formats. For each phase setting only one set of g_m cells is turned on using the EN signal. For simplicity, let's consider the clockwise set to understand the operation of the NRPS. Applying a sinusoidal voltage to port 1, P_1, results in a counterclockwise relative phase rotation at the A, B, C, and D nodes (0°, 90°, 180°, and 270°), mandated by the differential hybrid coupler. The g_m cell placed between nodes D and A, has an input and output voltage of V_D and jV_D and an output current of g_mV_D. Consequently, the equivalent impedance of this g_m cell is $\frac{+j}{g_m}$, presenting an inductor with an inductance of $\frac{1}{g_m\omega}$, where ω is the angular frequency. The same is true for all g_m cells due to circular symmetry. Similar to the RTPS shown before, this configuration imparts a forward

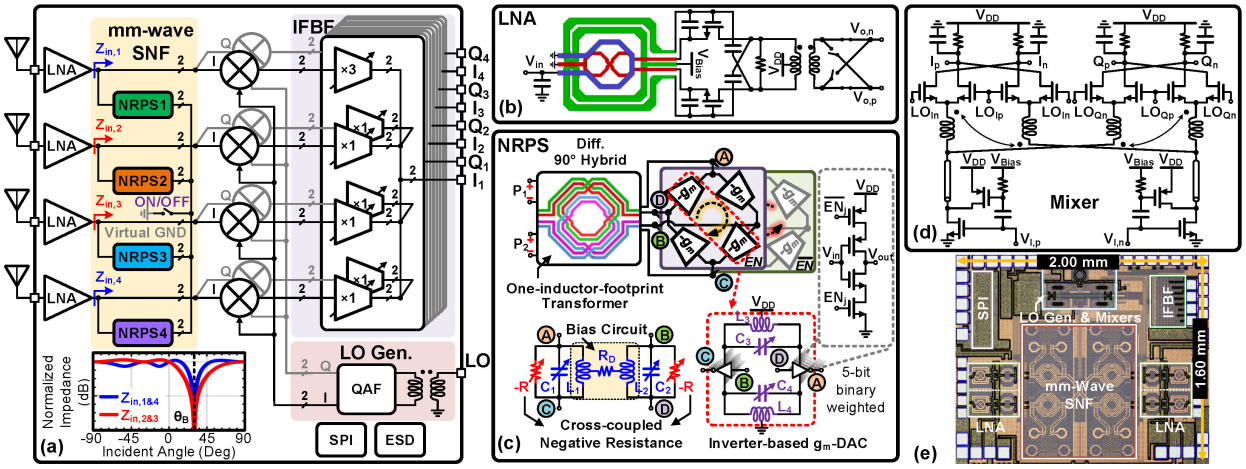

Fig. 5. (a) Block diagram of the implemented 4-element blocker-tolerant mm-wave MIMO RX and the simulated impedances, $Z_{in,1-4}$, seen from the SNF. Schematic of (b) the LNA with input passive components, (c) the low-loss NRPS with bias circuitry, and (d) the quadrature mixer. (e) Die micrograph.

phase-shift of $90^\circ + \alpha$, where α is $2\tan^{-1}(z_0 g_m)$ and z_0 is the characteristic impedance of the hybrid coupler (Fig. 4(b)).

Similarly, when a sinusoidal voltage is applied at P_2, a clockwise phase rotation is observed (in which D, C, B, and A relative phases are 0°, 90°, 180°, and 270°) as shown in Fig. 4(c). Following the same steps, the equivalent impedance is calculated as $\frac{-j}{g_m}$, functioning akin to a capacitor with a capacitance of $\frac{g_m}{\omega}$. This configuration imparts a reverse phase shift of $90^\circ - \alpha$ resulting in a nonreciprocal phase shift. As can be seen here, by using the clockwise set of g_m cells, a forward phase shift of $> 90^\circ$ and a reverse phase shift of $< 90^\circ$ can be achieved. The counter-clockwise set of g_ms can enable the opposite, therefore, increasing the NRPS coverage.

III. Circuit Implementation

The receiver block diagram is presented in Fig. 5(a). The main path of each element consists of an LNA, I/Q mixer and IF beamformer (IFBF). The impedances presented at the output of the LNAs, $Z_{in,1-4}$, when the NRPSs are tuned to reject a blocker at θ_B are shown in Fig. 5(a). The low impedances at the blocker angle effectively reduce the voltage swing at the output of the LNA. The LNA schematic is shown in Fig. 5(b). Since blockers are canceled at the output of the LNA, a single-stage LNA allows to have no internal nodes experiencing large blocker voltage swings causing inter-stage saturation. At the output of the LNA, a double-pole double-throw switch is employed to invert the polarity and to enable blocker rejection across the entire field-of-view.

NRPSs tap from each LNA output and connect to a central node. The differential S-parameter matrix of NRPS is given by:

$$S_{NRPS} = \begin{bmatrix} 0 & je^{-j\alpha} \\ je^{+j\alpha} & 0 \end{bmatrix} \quad (3)$$

The input impedance seen from the NRPS is $Z_{in} = \frac{z_0^2}{Z_L}$, where Z_L is the load impedance of the NRPS. When the second port of the NRPS is connected to ground, the input impedance goes toward infinity, presenting an open circuit. This implies that, in the absence of blockers within the electromagnetic environment, the NRPSs can be deactivated by connecting their common node to virtual ground (to not alter biasing) as depicted in Fig. 5(a), thereby reducing RX power consumption and NF by 16mW and 1.3dB, respectively. Fig. 5(c) provides the NRPS schematic. For the same current budget and in the absence of no voltage swing at the g_m cell outputs, complementary g_m cells offer higher transconductance and better linearity performance in comparison with NMOS-only ones. In this architecture, it can be shown that the amplified blocker signal appears at the common central node of the SNF. However, not all of the internal nodes of the NRPS see this voltage swing. *In fact, within the NRPS, blockers are only present at nodes A/C or B/D depending on the rotational configuration of g_m cells and there is minimal voltage swing at the alternate nodes (B/D or A/C).* In such a scenario, an inverter-based g_m cell proves to be an excellent choice to preserve NRPS linearity. 5-bit inverter-based g_m DACs are employed to adjust the phase-shift of NRPS. Inductors L_1 and L_2 alleviate the impact of parasitic capacitors and establish the bias for the NRPS. Cross-coupled inverters are used in the NRPS to create artificial negative resistors to minimize insertion loss. Additionally, capacitors C_3 and C_4 mitigate the impact of gate parasitic resistors. The differential hybrid coupler is implemented using a one-inductor-footprint transformer. Finally, since the blocker signal appears at the

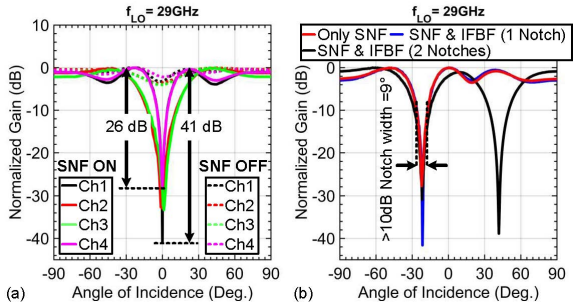

Fig. 6. (a) Measured in-band normalized gain versus angle of incidence for different channels. (b) Measured multi-blocker rejection.

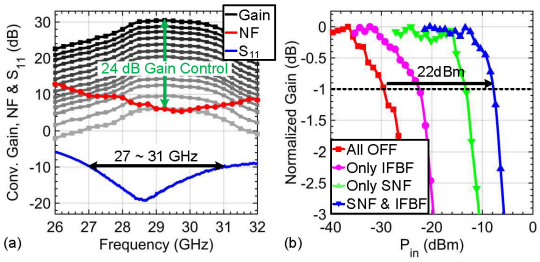

Fig. 7. (a) Measured single-element conversion gain, NF, and S_{11}. (b) Measured in-notch IP1dB for a notch at θ_B =-21°

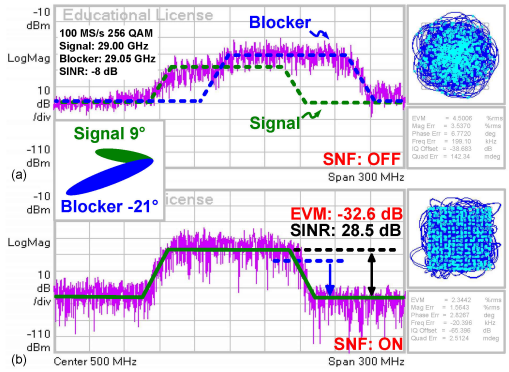

Fig. 8. Modulated measurements of the RX with SNF: (a) off and (b) on.

common node, an autonomous notch-steering loop can be implemented by using a voltage/phase detector similar to [4].

The quadrature mixer schematic is shown in Fig. 5(d), which benefits from a g_m-boosting and inductive peaking techniques to enhance the linearity performance. A quadrature all-pass filter is used to generate quadrature LOs for the mixers. Furthermore, the RX incorporates an IFBF to further enhance the notch depth or create a second notch.

IV. Measurement Results

The proposed RX is implemented in a 45nm SOI technology with an area of 3.2mm^2, as depicted in Fig. 5(e). A high-speed arbitrary waveform generator (AWG), Keysight M8194A, is employed to generate the mm-wave input signals. Fig. 6(a) depicts the normalized measured RX gain vs. angle of incidence when the SNF is on/off revealing a maximum notch depth of 41dB. In Fig. 6(b), the IFBF is configured to either deepen the notch created by the mm-wave SNF or create a second spatial notch. Additionally, a >10dB notch width of 9° is observed in the measurements. Fig. 7(a) shows the measured single-element gain, NF and S_{11} of the RX for a notch at 0°, achieving a gain range of 6-30dB and a minimum NF of 5.4dB. *The measured in-notch IP1dB, as shown in Fig. 7(b), demonstrates a notable improvement by utilizing both the SNF and IFBF, increasing from -29.5dBm to -7.8dBm.*

Two 100MS/s 256QAM modulated signals (at desired and blocker spatial angles as shown in Fig. 8(a)) with a 50% bandwidth overlap are applied at the receiver with an input Signal-to-Interference-plus-Noise Ratio (SINR) of -8dB. As can be seen in Fig. 8(b), turning on the SNF suppresses the blocker and improves the Error Vector Magnitude (EVM) to

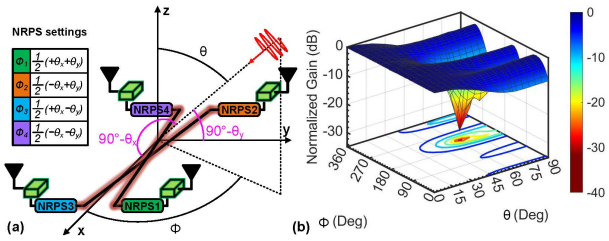

Fig. 9. (a) Configuration of the RX for 2-D SNF. (b) Normalized measured gain vs θ and ϕ for 2-D SNF.

Table 1. Performance summary and comparison with state-of-the-art receivers.

	M. Huang, TMTT19 [2]	M. Huang, JSSC19 [3]	R. Garg, ISSCC20	L. Zhang, ISSCC22 [4]	T. Huang, TMTT23	This Work
Technology	130nm SiGe	45nm SOI	65nm	40nm	45nm SOI	**45nm SOI**
Frequency Range [GHz]	23-30	27-41	28	23-29	23-37	**27-31**
Conversion Gain [dB]	33	36	>16	30	29.5	**30**
Spatial Blocker Suppression Dimension	1-D	1-D	1-D	1-D	2-D	**1-D and 2-D**
No. of Inputs/Outputs	8/2	4/4	4/4	4/4	4/4	**4/4**
N-Input N-Output SNF	No	Yes	Yes	Yes	Yes	**Yes**
Spatial Order of Notch	2 (Fixed)	4 (Scalable)	4 (Scalable)	4 (Scalable)	4 (Scalable)	**4 (Scalable)**
$NF_{DSB,eq}$ [dB]	4.2-6.3	4.3-6.3	6.0-7.8	4.8-7.1	4.8-5.9	**5.4-9.7**
In-Notch IP1dB [dBm]	N/A	-19[1]	N/A	-14	-20[1]	**-7.8**
Out-of-Notch/In-Notch OIP3 [dBm]	N/A	9/27	N/A	N/A	N/A	**14.1/30.1**
Max RF/IF Notch Depth [dB]	41	62	37	40	43.6	**41**
Min >10dB Cancellation Spatial Notch width [°]	48-58[1]	27-32[1]	~11 (CH1&4)[1] ~22 (CH2&3)[1]	8.5-14 (CH1&4) 22-24 (CH2&3)	28-51[2]	**8.7-13 (CH1&4) 23-25 (CH2&3)**
Power Cons./RX element [mW]	70	70-85	112.4	56.1	132.2-200.3	**62.8-71.4**
Modulation	100 MS/s 256 QAM	100 MS/s 256 QAM	100 MS/s 16 QAM	100 MS/s 64 QAM	100 MS/s 64 QAM	**100 MS/s 256 QAM**
Blocker/Signal Frequency Offset / Modulation BW	100%	50%	N/A	50%	50%	**50%**
Desired Signal EVM after Blocker Suppression [dB] (Input SINR [dB])	-32.6 (-10)	-32.8 (-8)	-20.3[3] (0)	-27.9 (-15)	-26.3[1] (-3[1])	**-32.6 (-8)**
Area [mm^2]	21.6	23.4	10.6	2.8	18.4	**3.2**

[1] Estimated from figures. [2] Calculated the real angles from figures. [3] Over-the-air (OTA) measurement results.

-32.6dB. Additionally, this design is capable of functioning as a 2-D 2×2 SNF, as illustrated in Fig. 9(a). The normalized gain, with a 30dB notch depth, is depicted versus θ and ϕ in Fig. 9(b), where θ and ϕ represent the angles in a spherical coordinate system within three-dimensional space.

V. Conclusion

This work presents a highly-linear blocker-tolerant mm-wave MIMO receiver that incorporates an SNF early in the RX chain to improve RX linearity and dynamic range with respect to spatial blockers. The SNF employs low-loss NRPSs in auxiliary paths. Measurements confirm the effectiveness of the proposed RX with an in-notch IP1dB value of -7.8dBm.

References

[1] L. Zhang et al., "Scalable Spatial Notch Suppression in Spatio-Spectral-Filtering MIMO Receiver Arrays for Digital Beamforming," *IEEE J. Solid-State Circuits*, vol. 51, pp. 3152–3166, Dec. 2016.

[2] M. Huang et al., "A Full-FoV Autonomous Hybrid Beamformer Array with Unknown Blockers Rejection and Signals Tracking for Low-Latency 5G mm-Wave Links," *IEEE Trans. Microw. Theory Techn.*, vol. 67, pp. 2964–2974, Jul. 2019.

[3] M. Huang and H. Wang, "A Mm-Wave Wideband MIMO RX with Instinctual Array-Based Blocker/Signal Management for Ultralow-Latency Communication," *IEEE J. Solid-State Circuits*, vol. 54, pp. 3553–3564, Dec. 2019.

[4] L. Zhang and M. Babaie, "A 23-to-29GHz Receiver with mm-Wave N-Input-N-Output Spatial Notch Filtering and Autonomous Notch-Steering Achieving 20-to-40dB mm-Wave Spatial Rejection and -14dBm In-Notch IP1 dB," in *IEEE ISSCC*, 2022, pp. 82–84.